Original Article

Axial strength of Zircaloy-4 samples with reduced thickness after a simulated loss of coolant accident

Jean Desquines[*], Tatiana Taurines

IRSN (Institut de Radioprotection et de Sûreté Nucléaire), PSN-RES, Saint Paul-Lez-Durance, 13115, France

ARTICLE INFO

ABSTRACT

To investigate wall-thinning impact on axial load resistance of Zircaloy-4 cladding rods after a LOCA transient, axial tensile samples have been machined on as-received tubes with reduced thicknesses between 370 and 580 μm. After high temperature oxidation under steam at 1200 °C with measured ECR ranging from 10 to 18% and water quenching, machined samples were axially loaded until fracture. These tests were modeled using a fracture mechanics approach developed in a previous study. Fracture stresses are rather well predicted. However, the slightly lower fracture stress observed for wall-thinned samples is not anticipated by this modeling approach. The results from this study confirm that characterizing the axial load resistance using semi-integral tests including the creep and burst phases was the best option to obtain accurate axial strengths describing accurately the influence of wall-thinning at burst region.

1. Introduction

During a LOCA, the fuel cladding deforms by internal pressurization inducing ballooning and can lead to burst during the heat up of the first phase of the LOCA. This phase is followed by high temperature oxidation under steam environment and then the rod is quenched during core reflooding.

The axial strength of a nuclear fuel cladding during the core reflooding is a key issue for safety evaluation [1—8]. It is usually considered that the cladding is subjected to an axial load during the quench. This load results from restraint displacement induced by grids and guide tubes [3].

Loading the rod during quench can lead to cladding fracture [4—9]. Such fractures are usually observed at the ballooned region where the cladding bursts but also sometimes at the secondary hydriding regions. In these deformed regions, the cladding thickness is strongly reduced by the ballooning phase before burst. To assess the resistance to axial load of the deformed and high temperature oxidized rod, one can evaluate the Equivalent Cladding Reacted (ECR) describing the fraction of oxidized cladding during steam oxidation.

There are several possible correlations used to assess the ECR

value: the Cathcart-Pawel correlation [10] is expected to provide best-estimate values between 1000 °C and 1200 °C and the Baker-Just correlation [11] leads to rather conservative ECR at these elevated temperatures. In France, for safety assessments, a critical ECR is defined depending on initial hydrogen content [1,2]. For a given exposure to steam, due to the locally reduced wall thickness, and two-sided oxidation at burst location the ECR is larger than anywhere else along the fuel rod.

The relevance of ECR as a scoping parameter indexing the resistance of a highly deformed cladding under axial load was established for transient heating burst tests by Chung and Kassner [12] for thermal shock failures during quench and handling failures, i.e. without significant external load. This parameter was also evaluated at JAEA during semi-integral thermal shock tests [4—9] leading to a boundary between failed and non-failed samples. But during these two types of tests, the failure is governed by a combination of complex parameters: hoop strain, secondary hydriding, failure during the quench and not necessarily at room temperature and possibly other structural effects. Actually, these tests are affected by azimuthal variation of strain and cladding temperature resulting from unperfect alumina pellets stacking [13]. It is considered by authors that the relevance of ECR to establish the failure limits has to be verified using dedicated experiment. This is the key issue of the present paper. The study also covers the influence of wall thinning induced by cladding corrosion during in reactor operation. Cladding tubular samples are thinned by turning

* Corresponding author.
  E-mail address: jean.desquines@irsn.fr (J. Desquines).

samples and removing part of the metallic thickness of the sample. The remaining metallic thickness represents that of a possibly corroded rod after the burst phase of a LOCA transient. This controlled wall thinning is used to evaluate the influence of a tube deformation and corrosion induced wall thinning on the ECR at fracture after a laboratory simulated LOCA.

This test series follows two other studies, one addressing the influence of hydrogen content [14] and the other the influence of one-sided versus two-sided oxidation [15]. These tests are used to compare the results on thinned wall samples and as-received ones.

2. Materials and methods

2.1. Material

Stress Relieved Annealed (SRA) low-tin Zry-4 with nominal chemical composition described in Table 1 is used in this study. The alloy was manufactured by CEZUS. The outer diameter of the tubes is 9.5 mm and the cladding thickness 0.57 mm.

2.2. Specimen preparation

The tube thinning was performed by turning the 72 mm long samples removing up to about 200 μm of the tube thickness. Some preliminary validation tests were separately performed to verify that sample turning didn't affected high temperature oxidation kinetics. Geometrical characterization of turned tubes was performed after wall thinning. After turning, the sample thickness versus azimuth followed a sinusoidal trend due to the small misalignment of turning axis. The sample legs were machined, using spark machining, at azimuths corresponding to comparable wall thickness at the two opposite azimuths. The final sample geometry is illustrated in Fig. 1. Spark machining scraps were used to measure the post-machining sample legs thickness as illustrated in Fig. 1.

After machining, a B-type thermocouple is spot welded on the upper region of the sample located between the sample legs. The B-type thermocouples contain Pt and a Zr–Pt eutectic might form at elevated temperature. As a result, the thermocouples might have a metallurgical influence on the sample. Consequently, the location to weld the B-type TCs was chosen in a region associated to very low stresses during mechanical testing.

In order to limit the temperature overshoot induced by the oxidation generated heat, after TC welding, the samples were pre-oxidized during 3 days at 470 °C under air environment. This pre-oxidation temperature is sufficiently low to avoid sample nitriding (this was confirmed by dedicated measurements) and sufficiently high to generate the pre-oxide layer within a short oxidation period. The pre-oxidation forms a 2.5 μm thick layer. This thickness corresponds to the one formed at 1200 °C after heating a bare cladding at 200 °C/s using the relevant Cathcart-Pawel correlation [10]. Additionally, this pre-oxidation layer is partly dissolved during the ~25 s heat-up phase and the maximum delay to re-start oxidation is shorter than 10 s [16]. This technique is considered as a good strategy to control both temperature overshoot and oxide layer thickness formed during the heat-up phase.

Table 1
Ingot measured chemical composition of the tested SRA Zry-4.

Sn (wt%)	Fe (wt%)	Cr (wt%)	O (wt%)	H (wppm)
1.30 ± 0.01	0.22 ± 0.01	0.11 ± 0.01	0.13 ± 0.01	7

2.3. Testing protocol

To evaluate the influence of cladding wall thickness on its axial resistance during LOCA core reflooding, the experiments consist in the following sequence:

- machining axial tensile sample with reduced wall thickness,
- sample preparation for high temperature oxidation (thermocouple welding, air pre-oxidation to prevent temperature overshoot, mounting alumina centering parts),
- high temperature steam oxidation ended by water quench consisting in dropping the sample in a water bath,
- mechanical testing of the sample at room temperature to characterize its axial strength after high temperature oxidation,
- post-test analysis.

The samples mass is systematically measured at each step having an influence on this parameter including thermocouple welding.

The experimental testing sequence before post-test characterization is illustrated in Fig. 2.

To anchor the sample during high temperature oxidation, a hollow alumina rodlet that can be moved axially in the furnace, upwards and downwards, is inserted at its lowest position (see Fig. 2). Two TC-wires are inserted within the alumina rodlet and finally coiled around the corresponding wire end of the sample welded B-type thermocouple to monitor and record temperature. When the samples are connected, the alumina rod is moved upwards to locate the axial tensile sample at the maximum temperature location within a 100-120 mm-long uniform temperature zone.

2.3.1. High temperature steam oxidation

The high temperature furnace is an electrically heated vertical furnace. A mixture of argon and overheated steam is supplied by the upper opening of the furnace (Fig. 2-c). 500 g/h of water and 600 Nl/h of argon are inserted corresponding to a 50%–50% volume mixture of water and argon fraction. The steam flow rate normalized to the cross-sectional area of the furnace alumina tube was 19.6 mg cm^{-2} s^{-1}, this flow rate being well above steam starvation conditions. When the sample is inserted, the oxidation duration measurement is triggered and, when reaching the expected exposure, the alumina rodlet maintaining the sample is released and the sample falls into a water bath located under the lower opening of the furnace as illustrated in Fig. 2. Depending on the chosen container for the water bath, the sample quench can be video recorded. During the present testing campaign a 5 L water bath was chosen and its temperature remained below 40 °C.

A typical temperature record obtained oxidizing a slightly pre-oxidized sample at high temperature is illustrated in Fig. 3. The oxidation experiment duration is considered to start at a temperature of ~15 °C before reaching the maximum temperature. The T_{max}-15 °C value is reached at a fast heating rate, leading to negligible growth of α(O) and ZrO_2 layers during the heat-up compared to the values obtained at the end of the oxidation test. This ΔT value also corresponds to the order of magnitude of the temperature decrease after reaching the T_{max} value. The water quenching leads to about 200 °C/s measured cooling rates. Consequently, the temperature record provides an extremely accurate time for the end of the oxidation period. The oxidation duration is considered to be: $t_{ox} = t_{end} - t_{start}$. The average temperature is calculated during t_{ox}: $T_{ox} = \int_{t_{start}}^{t_{end}} T(t)dt/t_{ox}$.

After high temperature oxidation, the sample outer radius was measured at mid-height of the sample legs using a Keyence laser
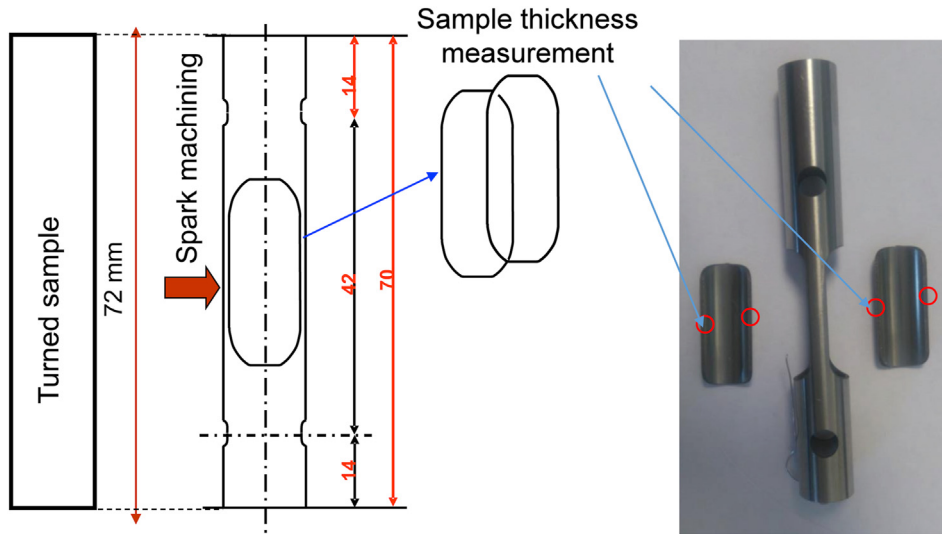
Fig. 1. Axial tensile sample geometry and spark machining scraps used for local thickness measurement.
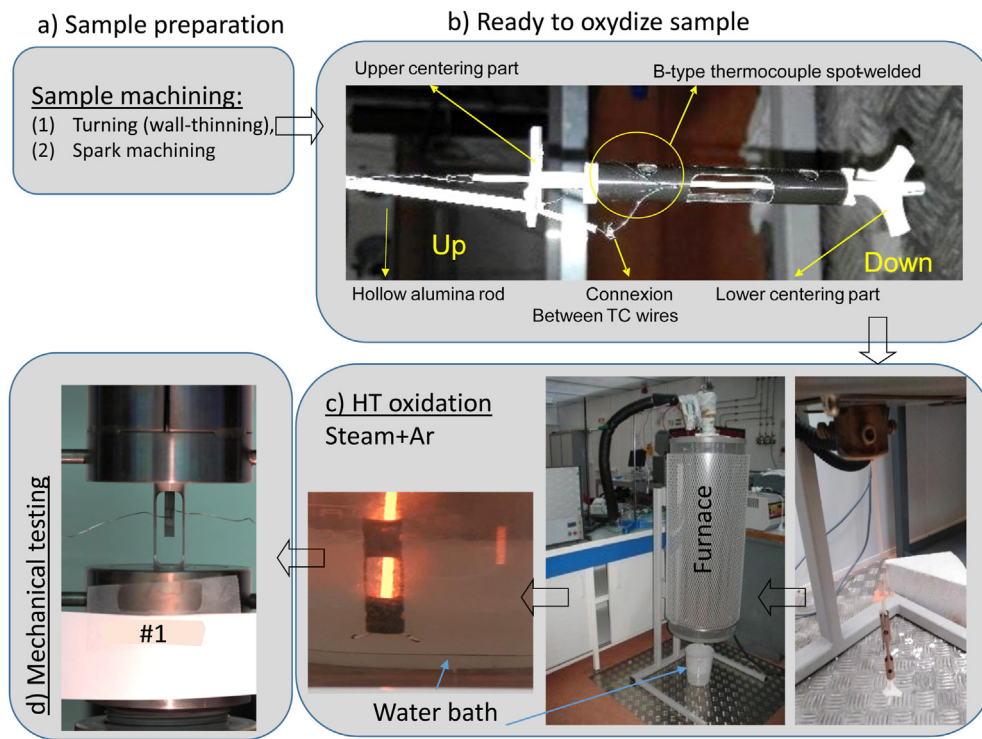

Fig. 2. Testing sequence to evaluate the influence of wall thinning.

micrometer having a 1.5 μm accuracy without any contact to the sample.

2.3.2. Sample mechanical testing

After high temperature oxidation, the samples are mechanically tested using an INSTRON 5566 electromechanical testing device with a 5 kN load cell. The samples are mounted using pin-loading and dedicated grips connected to the loading device. Then, a 1 mm/min displacement ramp is applied until sample fracture. The corresponding load at fracture is a key outcome that is also transformed into average axial stress in the axial tensile sample gauge section.

The fracture stress, σ_F, is the ratio between the obtained fracture load and the oxidized sample gauge section.

Very thin samples had a strong propensity to fail at pin holes. In this situation, usually corresponding to very high ECR, the tests cannot be used to determine the fracture load and are dismissed.

2.3.3. Metallography of a failed leg of the sample

A failed leg of the sample, and preferentially the one corresponding to the first fracture, is cut, embedded in a conductive resin and further prepared for metallographic examination. The thicknesses of the various observed layers, including: oxide, α(O), prior-β measured using optical microscopy with measurement accuracy of
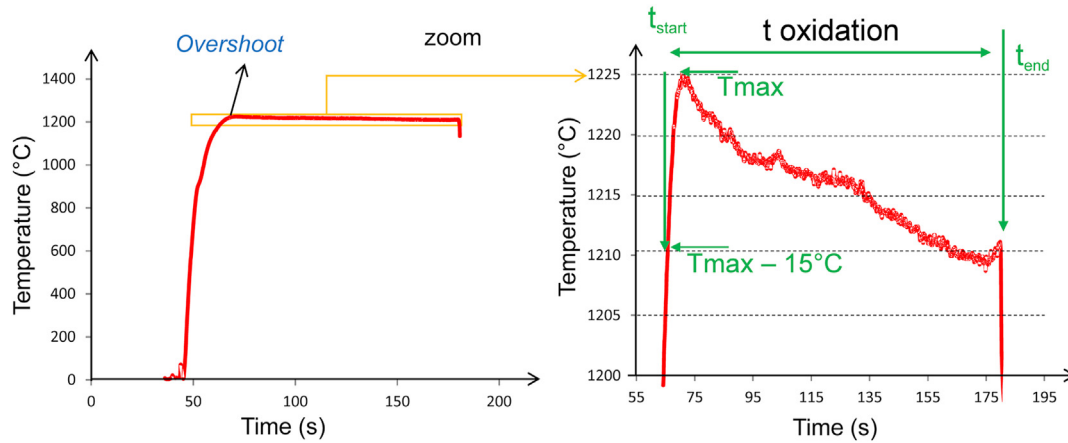
Fig. 3. Thermocouple temperature record and high temperature oxidation duration.

1—2 μm. For the oxide layers and the α(O) layers, the outer and inner thicknesses were very close and an average value of four measurements at outer surface and four others at inner surface was considered.

The α(O) phase fraction in the metallic part of the cladding was derived straightforward from scale thickness measurement, $f_\alpha = 2e_{\alpha(O)}/(2e_{\alpha(O)} + e_{prior-\beta})$, because no prior-β embedded α(O) inclusions were observed in any of the metallographic examinations.

2.3.4. Hydrogen content measurement

The remaining leg of the high temperature oxidized sample was used to measure hydrogen content using a LECO ONH-836. The measurement is first made keeping the oxide layers during measurement. Afterwards, using oxide layer thickness measurement, assuming no hydrogen remains in the oxide layers, the reference sample mass is corrected to determine the average hydrogen content in the metal.

2.4. Test matrix

The primary objective of the study was to test samples with 10—18% Cathcart-Pawel-ECR [10] obtained by 1200 °C two-side steam oxidation being in the order of magnitude of safety range [2].

The measured ECR is given by the ratio the mass change and its maximum possible value: $ECR = \frac{\Delta m}{2\frac{M_O}{M_{Zr}}m_0}$. Using this measurement means that the entire set of surfaces of the sample are taken into account as contributors to the ECR including inner and outer surface but also sample edges resulting from sample machining.

At the end, 19 samples were successfully tested with wall thinning comprised between 0 and 200 μm. Each of these tested samples is mentioned in Table 2 and the associated measured ECR based on weight gain is given. The maximum wall thinning of 200 μm corresponds to a ballooning deformation of 54% which is larger than the order of magnitude of measured ballooning strains

after testing irradiated rodlets under LOCA conditions [14], in the JAEA semi-integral tests (maximum strain of about 40%). The studied range also covers the possible influence of wall thinning induced by cladding corrosion during normal in-reactor operation.

3. Results

3.1. Main measurements

The oxide layer thicknesses were measured using r-z metallographic cut along a leg, it is impossible to distinguish the inner surface and the outer surface. The average oxide layer along the
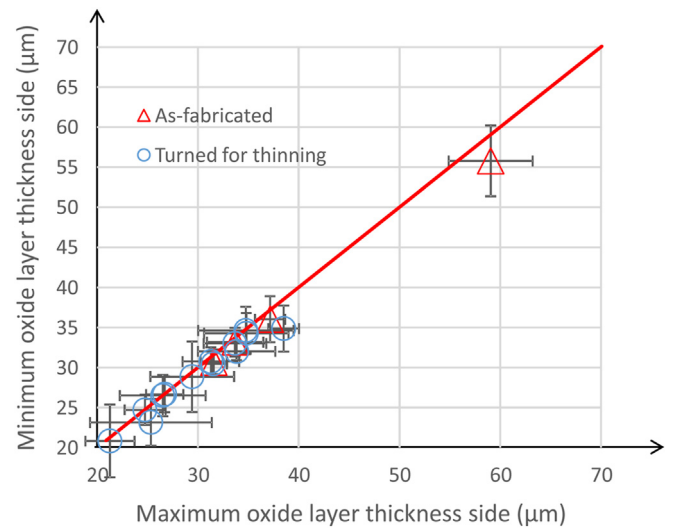

Fig. 4. Minimum oxide layer thickness versus maximum with two standard deviations uncertainty.

Table 2
Test matrix.

Wall thinning (μm)	0	50	100	150	200
#Test ID (Measured ECR%)	#02(11,7%)				
	#04(10,7%)				
	#05(10,7%)	#29(11,3%)		#13(11,7%)	
	#06(18.9%)	#30(11,1%)	#08(12,8%)	#14(12,0%)	
	#23(18,0%)	#31(10,6%)	#10(11,0%)	#15(10,2%)	#19(10,1%)
	#25(11,9%)	#32(11,1%)	#35(9,4%)	#16(10,3%)	#37(11,1%)

side with maximum average oxide layer thickness is compared to the side with minimum average oxide layer thickness in Fig. 4. It appears in this plot that there is no clear difference in the oxide layer thickness between inner and outer diameter for as-fabricated and turned samples. This confirms that turning has no adverse effect on oxidation kinetics. Consequently the average oxide layer thickness on both sides is considered in the following. Spark machining used to machine the samples legs was verified to have no impact on the leg edges oxide layer at 1200 °C since the oxide layer thicknesses at the inner and the outer surface are similar up to very high measured ECR values (above 18%).

All the tested samples were brittle, generating no plastic strain as illustrated in Fig. 5 for sample #5 leading to the highest fracture stress within the test matrix. The typical load-displacement record consists in a short period during which the gaps between the loading pins and the sample are progressively closed and then the elastic slope of the sample appears up to sample failure.

The main test results are summarized in Table 3. e_0 is the sample thickness measured after wall thinning. The average high temperature steam oxidation T_{ox} and exposure t_{ox} are also indicated in Table 3.

Table 3 provides the post-oxidation external radius influenced by oxidation induced swelling (R_e), the metallic content of hydrogen after high temperature oxidation ($[H]_{LT+HT}$) and the two standard deviations scatter on this measurement, the $\alpha(O)$ phase fraction within the metal (see Ref. [14] for the measurement techniques based on metallography), the ECR deduced from weight gain measurements, the axial fracture stress at the sample gage section (σ_F) and the normalized axial load at fracture extrapolated to the section of a full cylinder (F/rod = $\sigma_F.S_{rod}$). It is worth reminding that the samples systematically failed in the brittle range generating non measurable plastic deformation.

All these parameters contribute to a better understanding of the tests. Assuming all the hydrogen content is localized in the prior-β phase, this local hydrogen content can be assessed using the following equation:

$$[H]_{prior-\beta} = [H]_{LT+HT} / (1 - f_\alpha) \qquad (1)$$

It was shown in two previous studies [14,15] that the sample behaves during the mechanical testing as a pre-cracked tube. Indeed during the early phases of the mechanical test two opposite cracks are nucleated at inner and outer cladding surface with crack depth (a) corresponding to the cumulated depth of $\alpha(O)$ and zirconia layers:

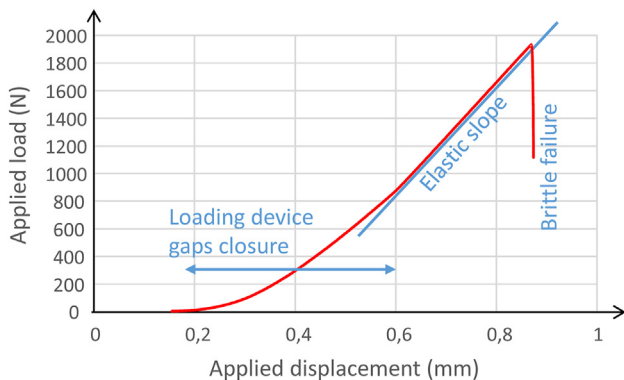$$a = e_{ZrO_2} + e_{\alpha(O)} \qquad (2)$$

Fig. 5. Load displacement record of test #05 loaded at 1 mm/mn and leading to a brittle failure.

This situation is illustrated in Fig. 6 showing the metallography of a sample that was oxidized at elevated temperature and subjected to ring compression test leading to a ductile failure. The ductility promotes multiple crack nucleation as observed in this figure and facilitate evidencing incipient cracks. The oxygen enriched α layer is better evidenced by the incipient crack penetration into the metal rather than by the bright aspect obtained by the polishing process. Usually when testing a very brittle material a single crack is nucleated. This is the situation of the axial tensile tests performed in the present study, and the incipient crack belongs to the failure path and consequently cannot be observed.

The crack tips are located at the interface of the α(O) and prior-β phases. At this location, in the prior-β side of the interface, the phase diagram establishes a link between hydrogen content and oxygen content. The fracture toughness of the sample can consequently be indexed only on hydrogen content, considering oxygen is at equilibrium content. The dependence of fracture toughness with prior-β phase hydrogen content, $[H]_{prior-\beta}$, is described in Refs. [14,15].

3.2. Fracture load and measured ECR fracture diagram

The test results obtained in the present study were combined with complementary results from past programs ([14—18]) using as-received Zircaloy-4 axial tensile samples with nominal thickness (570 μm). The entire set of results is plotted in Fig. 7-a in terms of fracture loads versus measured ECR. The measured ECR is expected to be comparable to the CP-ECR at 1200 °C steam oxidation. There is no doubt checking Fig. 7-b that the fracture load increases for thicker cladding. Fig. 7-b plots fracture load versus nominal cladding thickness for measured ECR values between 10 and 15%, it rather confirms the strengthening influence of the cladding thickness on the sample axial load resistance.

The axial fracture stress versus measured ECR is plotted in Fig. 8. The results in Fig. 8-b show a better independence to the cladding thickness compared to the axial load plot of Fig. 7-b. There is almost no influence of the cladding thickness on the measured fracture stress.

4. Discussion

The strategy of the present paper is to use very simple testing conditions that are expected to be activated locally during a semi-integral thermal shock test. Using simple sample geometry facilitates the understanding of the failure process and provides simple testing parameters such as: homogeneous temperature, simple stress field, uniform oxygen affected layers, locally constant ECR … The transposition of the results obtained using very analytical samples to semi-integral tests is out of the scope of the present study.

Using the axial tensile sample geometry of the present paper, the lateral edges of the sample are oxidized by the steam environment contributing up to about 16% of the sample surface. The resulting crack depth "a", is considered to be almost constant along the sample leg periphery. This oxidation is taken into account for ECR calculation by including the sample edges contribution to the weight gain. The stress intensity factor of an infinitely long surface crack contained in a semi-infinite body is: $K_I = 1.122.\sigma.\sqrt{\pi a}$. Consequently, for shallow surface cracks, crack nucleated along the sample edges have comparable influence than cracks nucleated along the sample-legs inner and outer surface. For deeper nucleated cracks the stress intensity factor is intensified by finite sample geometry for inner and outer surface cracks ($K_I = f\left(\frac{a}{e}\right).\sigma.\sqrt{\pi a}$, see the Tada & Paris handbook [19] for double edge cracked plate

Table 3
Main test results (nm: not measured).

Sample	e_0	T_{ox}	t_{ox}	e_{ZrO_2}	$e_{prior-\beta}$	$e_{\alpha(O)}$	R_e	$[H]_{LT+HT}$	fα	Mes. ECR	F/rod	σ_F
(#)	(μm)	(°C)	(s)	(μm)	(μm)	(μm)	(mm)	(ppm)	(%)	(%)	(N)	(MPa)
#02	580	1193	164	37	447	49	4.763	38 ± 13	18.0	11.7	7866	450
#04	580	1215	114	31	461	41	4.761	37 ± 12	15.0	10.7	7543	443
#05	580	1208	114	33	445	47	4.762	28 ± 3	17.6	10.7	8630	505
#06	580	1192	456	57	382	76	4.770	33 ± 8	49.0	18.9	4315	244
#23	573	1205	448	74	300	87	4.776	39 ± 13	nm	18.0	4020	229
#25	578	1215	161	44	408	52	4.766	35 ± 9	nm	11.9	7924	466
#29	533	1193	180	35	384	49	4.712	38 ± 12	20.2	11.3	7190	468
#30	533	1205	183	35	369	48	4.712	41 ± 16	20.7	11.1	6720	451
#31	527	1203	183	33	390	46	4.712	48 ± 23	19.2	10.6	7465	488
#32	535	1211	183	33	383	47	4.712	53 ± 28	19.7	11.1	7472	493
#08	486	1215	115	37	344	47	4.663	29 ± 3	21.5	12.8	4972	348
#10	487	1222	79	31	389	40	4.661	28 ± 2	16.9	11.0	6160	422
#35	483	1208	80	27	356	36	4.659	43 ± 17	17.6	10.7	6527	505
#13	442	1212	92	31	313	40	4.611	32 ± 7	20.4	11.7	4542	359
#14	438	1199	92	29	305	39	4.610	45 ± 19	20.3	12.0	4821	394
#15	435	1209	64	27	336	32	4.609	28 ± 2	15.9	10.2	5317	422
#16	442	1205	64	24	336	32	4.608	29 ± 3	16.0	10.3	6781	543
#19	389	1207	50	21	293	28	4.557	30 ± 5	15.8	10.1	4644	432
#37	390	1205	73	25	261	35	4.559	44 ± 19	20.4	11.1	4579	430
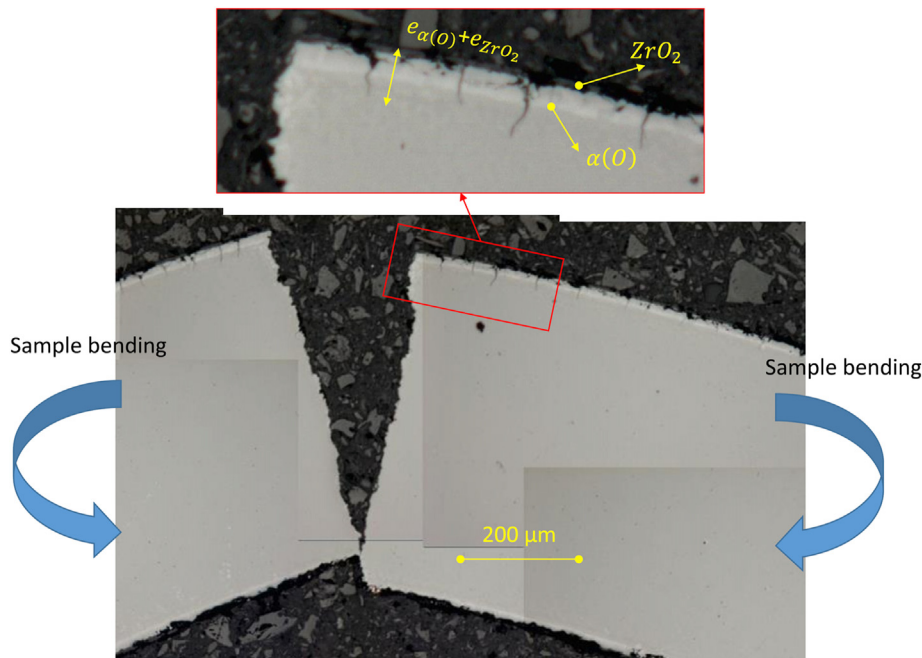
Fig. 6. Illustration of incipient crack nucleation of a high temperature oxidized sample subjected to ring compression test.

$f\left(\frac{a}{e}\right) = \dfrac{1.122 - 0.561\frac{2a}{e} - 0.015\left(\frac{2a}{e}\right)^2 + 0.091\left(\frac{2a}{e}\right)^3}{\sqrt{1-\frac{2a}{e}}}$, being an increasing function of $\frac{a}{e}$) but not to the same extent for edge cracks (for which $\frac{2a}{e}$ has to be modified into $\frac{2a}{W} \ll \frac{2a}{e}$ in the Tada & Paris equation, the maximum crack extension being the leg width: $\frac{W}{2}$). Consequently, the stress intensity factors are always comparable or stronger for inner and outer surface cracks rather than edge cracks. For failure modeling, the sample failure can be systematically considered as governed by inner and outer surface cracks rather than edge cracks.

The tests were modeled using a linear elastic fracture mechanics approach developed for axial tensile samples in Refs. [14,15]. The model leads to the following fracture stress:

$$\sigma_F = \frac{K_{Ic}\left([H]_{prior-\beta}\right)}{f\left(\frac{a}{e}\right)\sqrt{\pi a}} \tag{3}$$

$f\left(\frac{a}{e}\right)$: is the shape function determining the stress intensity factor of the tested sample with two opposite cracks nucleated within the sample legs inner and outer surfaces (see Ref. [15]).

The hydrogen content within the samples is assumed to correspond to the average value measured within the remaining metal after high temperature oxidation (see Table .3). The modeling results are compared to the experimental data in Fig. 9. The modeling expects a slight strengthening influence of wall thinning whereas the experimental data indicate almost no influence of wall
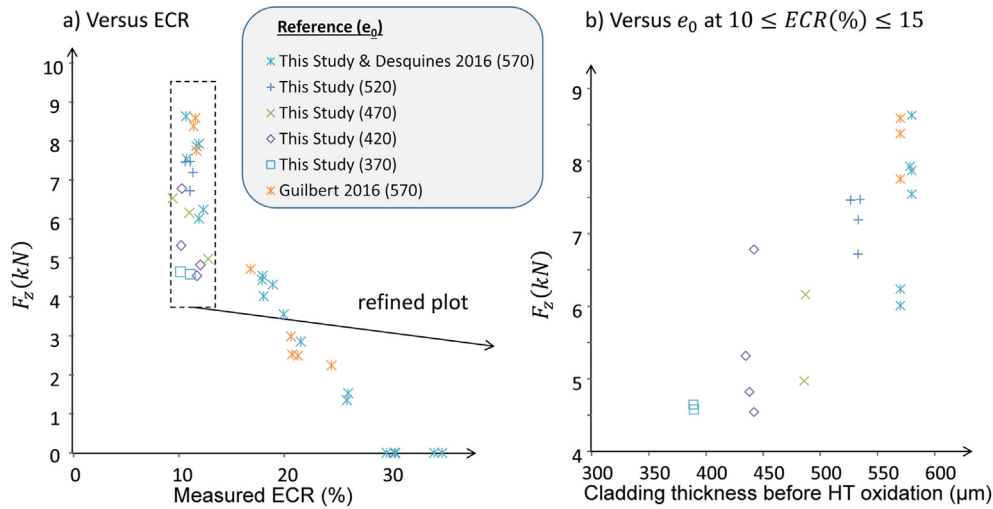
Fig. 7. Influence of wall thinning on the axial fracture load (left: versus measured ECR, right: versus cladding nominal thickness e_0).
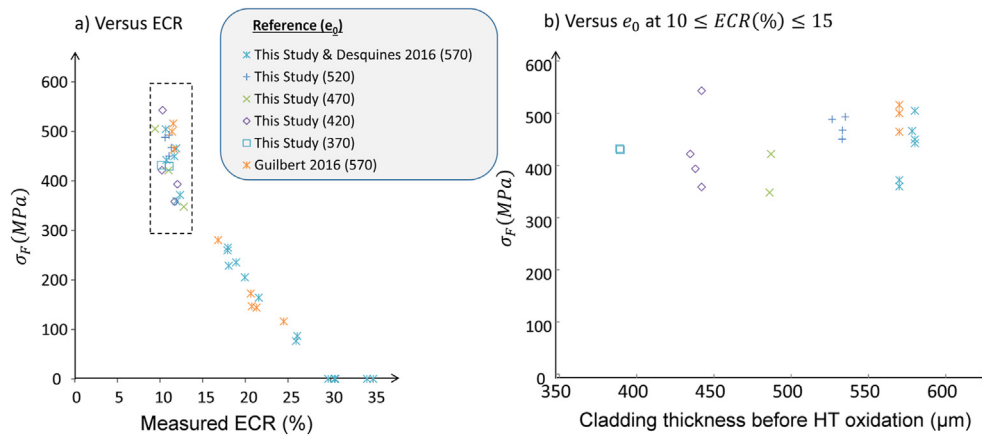

Fig. 8. Axial fracture stress versus measured ECR for sample having nominal thickness varying between 370 and 570 μm.
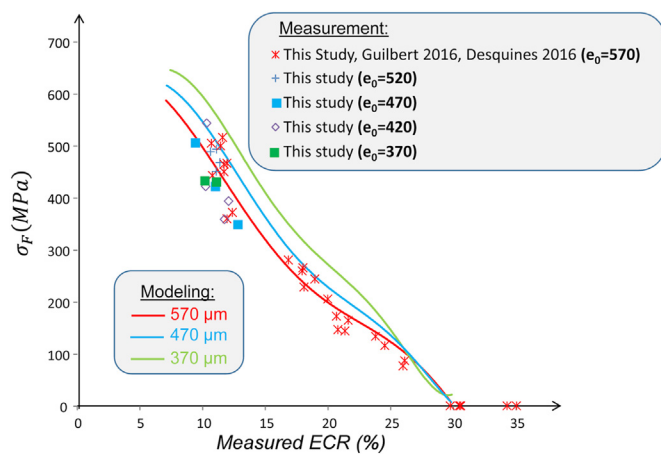

Fig. 9. Evaluation of the influence of wall thinning − comparison between test results and fracture mechanics modeling.

thinning. In spite of this difference, the modeling only slightly over-predicts the influence of wall thinning measured on the experimental data.

In the following a small analysis of the parameter helps to describe the expected influence of cladding thickness on the sample fracture stress.

In the brittle range, the fracture condition provided by equation (3) can be modified into:

$$\sigma_F = \frac{K_{Ic}}{f\left(\frac{a}{e}\right)\sqrt{\pi \frac{a}{e}}} \frac{1}{\sqrt{e}} \tag{4}$$

If we consider that during high temperature, a metal volume Ω is oxidized and transformed into Ω_{ox}. The oxygen concentration at $M_{ox} \in \Omega_{ox}$ is:$[O](M_{ox})$ and the material density depends on the local oxygen concentration: $\rho([O])$, being approximately ρ_{Zr} in the metal and ρ_{ZrO_2} in the oxide.

The ECR is defined as the ratio of the mass increase in the oxidized volume, Ω_{ox}, divided by the maximum possible mass increase of the original metal volume, Ω, as $ECR = \frac{\int_{M_{ox} \in \Omega_{ox}} [O](M_{ox})\rho([O](M_{ox}))d\Omega_{ox}}{[O]_{ZrO_2} \cdot \rho_{ZrO_2} \cdot \Omega.PB}$. The oxygen concentration at any location $M_{ox} \in \Omega_{ox}$ is $[O](M_{ox})$ and the local density of the material is $\rho([O](M_{ox}))$.

Assuming a linear oxygen distribution within the α-phase, varying between$[O]_{ZrO_2/\alpha(O)}$ and $[O]_{\alpha(O)/\beta}$, the ECR value can also be

evaluated with reasonable accuracy as:

$$ECR = \frac{\rho_{ZrO_2}.[O]_{ZrO_2}.e_{ZrO_2} + \rho_{Zr}\frac{([O]_{ZrO_2/\alpha(O)}+[O]_{\alpha(O)/\beta})}{2}.e_{\alpha(O)}}{\rho_{ZrO_2}.[O]_{ZrO_2}.\frac{PB.e_0}{2}} \quad (5)$$

$[O]_{ZrO_2}$: being the oxygen concentration in the zirconia (~27 wt%).

$[O]_{ZrO_2/\alpha(O)}$: is the oxygen concentration in the α(O) layer at the interface with the zirconia (about 7 wt%),

$[O]_{\alpha(O)/\beta}$: is the oxygen concentration in the α(O) layer at the interface with prior-β phase (about 2.5 wt%).

ρ_{ZrO_2} and ρ_{Zr}: are the densities of zirconia and zirconium (respectively: $5.82 g/cm^3$ and $6.55 g/cm^3$),

PB: is the Pilling-Bedworth ratio of zirconia (1.56).

It can be evaluated using Table 3 measurement, that: $e_{\alpha(O)} = 1.3 e_{ZrO_2}$.

Combining equations (2) and (5) leads to:

$$ECR = 0.84 \frac{a}{e_0} \quad (6)$$

Considering that a/e is very close to a/e_0, it can be deduced from eq. (6) that the ratio a/e is proportional to ECR and only depends on Zr−O−H phase diagram and zirconium physical properties. Considering eq. (4), the fracture stress is expected to mainly depend on ECR, sample thickness and material fracture toughness: $\sigma_F \sim g(ECR).\frac{K_{Ic}}{\sqrt{e}}$

This stress is expected to decrease with increasing cladding thickness as observed on the modeling. Additionally, the fracture toughness is expected to increase with decreasing sample thickness. No explanation could be found to explain the negligible influence of wall thinning observed during the performed tests. The temperature recorded by thermocouples might be slightly different from the one of the sample legs and this difference possibly depends on sample thickness. No difference in sample legs temperature is expected because the samples are positioned in the middle of the furnace section.

5. Conclusion

In the absence of a corrosion layer, a strengthening influence of increasing wall thickness on the axial fracture load was observed whereas almost no effect of wall-thinning on the fracture stress in the axial direction of a cladding was observed. The influence of wall thinning on a cladding mechanical resistance was both experimentally studied and compared to linear elastic based fracture mechanics modeling. The modeling slightly failed since when decreasing thickness a slight increase of fracture stress was predicted whereas no dependency to cladding thickness was experimentally observed. No clear explanation could be provided for this.

The axial load resistance during quench of ballooned semi-integral tests is, however, expected to be similar compared to an undeformed cladding with comparable ECR. Actually, assuming that ballooning is governed by plane strain deformation, the surface of the section of the tube remains unchanged at any axial location, and the applied stress is comparable whatever the deformation is. However, a fracture stress versus ECR fracture criterion appears to be better adjusted to the experimental data rather than an axial load versus ECR criterion.

Considering the influence of a corrosion layer, it cannot be concluded straightforward that the influence of a corrosion layer can be conservatively represented by wall thinning, because the oxide layer might have an influence on the sample fracture by contributing to incipient crack depth.

Therefore there is a need for separate effect studies addressing the influence of a pre-existing corrosion layer.

Declaration of competing interest

The authors declare that they have no known competing financial interests or personal relationships that could have appeared to influence the work reported in this paper.

Acknowledgements

References

[1] S. Boutin, S. Graff, "A new LOCA safety demonstration in France", Top Fuel meeting, 13-17, September, 2015.
[2] A. Cabrera, N. Waeckel, "A strength based approach to define LOCA limits", Top Fuel meeting, 13-17, September, 2015.
[3] K. Honma, S. Doi, M. Ozawa, S. Urata, T. Sato, Thermal-shock Behavior of PWR High Burnup Fuel Cladding under Simulated LOCA Conditions, ANS 2001 Annual Meeting, Milwaukee, Wisconsin, USA, 2001, pp. 17–21. June.
[4] F. Nagase, T. Fuketa, Effect of pre-hydriding on thermal-shock resistance of Zircaloy-4 cladding under simulated loss-of-coolant conditions, J. Nucl. Sci. Technol. 41 (7) (2004) 723–730.
[5] F. Nagase, T. Fuketa, Behavior of pre-hydrided Zircaloy-4 cladding under simulated LOCA conditions, J. Nucl. Sci. Technol. 42 (2) (2005) 209–218.
[6] F. Nagase, Fracture behavior of irradiated Zircaloy-4 cladding under simulated LOCA conditions, J. Nucl. Sci. Technol. 43 (9) (2006) 1114–1119.
[7] F. Nagase, T. Chuto, T. Fuketa, Behavior of high burnup fuel cladding under LOCA conditions, J. Nucl. Sci. Technol. 46 (7) (2009) 763–769.
[8] F. Nagase, Status and Plan of LOCA Studies at JAEA, Fuel Safety Research Meeting, Tokai, Japan, 2010, pp. 19–20. (Accessed May 2010).
[9] R. Thieurmel, J. Besson, E. Pouillier, A. Parrot, A. Ambard, A.-F. Gourgues-Lorenzon, Contribution to the understanding of brittle fracture conditions of zirconium alloy fuel cladding tubes during LOCA transient, J. Nucl. Mater. 527 (2019).
[10] J.V. Cathcart, R.E. Pawel, R.A. McKee, R.E. Druschel, G.J. Yurek, J.J. Campbell, S.H. Jury, Zirconium metal-water oxidation kinetics − IV Reaction rate studies, ORNL/NUREG, 17, August, 1977.
[11] L. Baker, L.C. Just, "Studies of metal-Water reactions at high temperature − III Experimental and theoretical studies of the zirconium-water reaction", ANL 6548 (1962).
[12] H.M. Chung, T.F. Kassner, Embrittlement criteria for Zircaloy fuel cladding applicable to accident situations in light-water reactors: summary report, January, 1980, pp. 45–47. NUREG/CR-1344, ANL, 79-48.
[13] T. Narukawa, M. Amaya, The effect of azimuthal temperature distribution on the ballooning and ruptuture behavior of Zircaloy-4 cladding tube under transient-heating conditions', J. Nucl. Sci. Technol. 53 (11) (2016) 1758–1765.
[14] J. Desquines, D. Drouan, S. Guilbert, P. Lacote, Embrittlement of pre-hydrided Zircaloy-4 by steam oxidation under simulated LOCA transients", J. Nucl. Mater., Volume 469, February, 2016, Pages 20-31.
[15] J. Desquines, S. Guilbert, T. Taurines, V. Busser, Fracture mechanics analysis of Zircaloy-4 tubular samples after laboratory simulated LOCA transients", Eng. Fract. Mech. 193 (2018) 96–107.
[16] J. Desquines, C. Duriez, S. Guilbert, T. Taurines, High temperature oxidation and room temperature axial strength of pre-oxidized zircaloy-4 cladding after a simulated LOCA", J. Nucl. Mater., volume 453, January, 2021.
[17] M. C. Billone, "Assessment of Current Test Methods for Post- LOCA Cladding Behavior" − NUREG-CR/7139 − 2012.
[18] S. Guilbert-Banti, J. Desquines, Fuel cladding post-quench LOCA embrittlement: mechanical test relevance, Top Fuel (2016) 11–15. Boise, ID. (Accessed September 2016).
[19] H. Tada, P.C. Paris, G.R. Irwin, The stress analysis of cracks Handbook, in: P. Production, St. Louis, USA, 1985.

GLOSSARY

a: incipient crack depth
Δm: mass change of the sample during high temperature oxidation

ECR: Equivalent Clad Reacted, the measured ECR deduced from weight gain measurement is defined as sample weight variation induced by oxidation normalized by its maximum possible value associated to fully oxidized sample- $\Delta m / \Delta m_{max}$ with $\Delta m_{max} = m.\frac{2.M_O}{M_{Zr}}$

e_0: cladding thickness after wall-thinning

e: cladding thickness after high temperature oxidation

$e_{\alpha(O)}$: oxygen enriched α layer thickness, average value for inner and outer diameter

$e_{prior-\beta}$: prior-β layer thickness

e_{ZrO_2}: zirconia layer thickness, average value for inner and outer diameter

f_α: α-phase fraction in the metal after high temperature oxidation

F_Z: fracture axial load by rod

g(ECR): is an arbitrary function

$[H]_{LT+HT}$: hydrogen content after high temperature oxidation

$[H]_{prior-\beta}$: prior-β layer hydrogen content, assumed to be equal to: $[H]_{prior-\beta} = [H]_{LT+HT}/(1-f_\alpha)$

HT: High Temperature

m: sample mass

m_0: mass of the sample before high temperature oxidation

M_O, M_{Zr}: respectively the molar mass of oxygen (16 g/mol) en zirconium (91.22 g/mol)

PB: Pilling-Bedworth ratio, corresponding in the context of zirconium alloys to the volume change converting zirconium into zirconia. This parameter is 1.56

ρ_{Zr}: is the density of zirconium (6.55g /cm^3)

ρ_{ZrO_2}: is the density of zirconia (5.82g /cm^3)

R_e: external radius of the HT oxidized samples

σ_F: fracture axial stress, determined as the ratio between fracture load normalized by oxidized sample gage section

TC: thermocouple

t_{ox}: steam oxidation duration

T_{ox}: steam oxidation average temperature

W: sample leg width (3 mm)

WG: Weight Gain